doi:10.1038/nature05935

LETTERS

Protective and therapeutic role for αB-crystallin in autoimmune demyelination

Shalina S. Ousman[1], Beren H. Tomooka[2,3], Johannes M. van Noort[4], Eric F. Wawrousek[5], Kevin O'Conner[6], David A. Hafler[6], Raymond A. Sobel[7], William H. Robinson[2,3] & Lawrence Steinman[1]

αB-crystallin (*CRYAB*) is the most abundant gene transcript present in early active multiple sclerosis lesions, whereas such transcripts are absent in normal brain tissue[1]. This crystallin has anti-apoptotic[2–7] and neuroprotective[8] functions. CRYAB is the major target of CD4$^+$ T-cell immunity to the myelin sheath from multiple sclerosis brain[9,10]. The pathophysiological implications of this immune response were investigated here. We demonstrate that CRYAB is a potent negative regulator acting as a brake on several inflammatory pathways in both the immune system and central nervous system (CNS). *Cryab*$^{-/-}$ mice showed worse experimental autoimmune encephalomyelitis (EAE) at the acute and progressive phases, with higher Th1 and Th17 cytokine secretion from T cells and macrophages, and more intense CNS inflammation, compared with their wild-type counterparts. Furthermore, *Cryab*$^{-/-}$ astrocytes showed more cleaved caspase-3 and more TUNEL staining, indicating an anti-apoptotic function of Cryab. Antibody to CRYAB was detected in cerebrospinal fluid from multiple sclerosis patients and in sera from mice with EAE. Administration of recombinant CRYAB ameliorated EAE. Thus, the immune response against a negative regulator of inflammation, CRYAB, in multiple sclerosis, would exacerbate inflammation and demyelination. This can be countered by giving CRYAB itself for therapy of ongoing disease.

Responses to injury often are accompanied by protective mechanisms that antagonize the damaging events or mediate repair. This is relevant in autoimmune demyelinating diseases such as multiple sclerosis, where the current and experimental treatment strategies aim to decrease the pathological immune activity in the CNS. We investigated whether CRYAB, a member of the small heat shock family of proteins, and a dominant target of the T cells in multiple sclerosis[9,10], with pro-survival[2–7] and anti-neurotoxic[8] properties, was protective in demyelinating disease.

EAE was examined in *Cryab*$^{-/-}$ mice immunized with myelin oligodendrocyte glycoprotein (MOG). These mice showed more severe clinical EAE, particularly at the peak and chronic phases of disease compared to 129S6 wild-type animals (Fig. 1a and Supplementary Table 1). This difference was associated with more severe inflammation and demyelination in the brain and spinal cord of *Cryab*$^{-/-}$ animals both in the acute (day 14) and progressive (day 42) phases of disease (Table 1 and Supplementary Fig. 1). To determine whether there was more cell death, which may have contributed to the worsened disease in *Cryab*$^{-/-}$ animals, we analysed brains and spinal cords from wild-type and *Cryab*$^{-/-}$ EAE mice for cleaved and uncleaved caspase-3. Cryab protects cells from apoptosis by down-regulating caspase-3 expression during stress[7,11]. Compared to wild-type animals, mice lacking *Cryab* expression had more staining for uncleaved caspase-3 in inflammatory lesions in the CNS, particularly in spinal cord at both the acute (day 14) (Supplementary Fig. 2) and later (day 42) stages (Fig. 1g, h) of EAE. Cleaved caspase-3 expression was only observed at day 42 in both wild-type and *Cryab*$^{-/-}$ mice with EAE (Fig. 1d–f and Supplementary Fig. 2). The *Cryab*$^{-/-}$ mice showed more staining of cells with large nuclei and abundant cytoplasm, which were morphologically consistent with glia in the white matter, whereas few smaller immune cells were positive (Fig. 1f). To correlate the cleaved caspase-3 expression with apoptosis, we performed TUNEL staining on CNS tissues of mice with late-stage EAE. Most TUNEL-positive cells in wild-type animals with EAE showed typical dense nuclear staining (Fig. 1i), whereas TUNEL-positive cells in the *Cryab*$^{-/-}$ mice were more numerous, and a greater proportion of positive cells had more abundant, diffuse cytoplasm staining and processes, suggesting that they were glia (Fig. 1j). We quantified the numbers of TUNEL-positive presumed immune cells (parenchymal nuclei) from apoptotic glial cells (Table 1). Null animals had more TUNEL-positive parenchymal and glial staining at both the acute (day 14) and progressive (day 42) EAE stages (Table 1). These results indicate that Cryab may have a role in preventing apoptosis of glial cells in the CNS during EAE.

EAE is driven by pathogenic immune responses against myelin proteins and lipids. Cryab may have an anti-inflammatory role[8]. To determine whether the immune response to constitutively expressed myelin proteins was also affected in *Cryab*$^{-/-}$ mice with EAE, we compared the proliferative ability and cytokine secretion of lymphoid cells from the spleen and lymph nodes from *Cryab*$^{-/-}$ and wild-type animals. Splenocytes and lymph node cells from *Cryab*$^{-/-}$ MOG-immunized mice showed significantly higher proliferation and secretion of the Th1 cytokines IL-2, IFN-γ, TNF, IL-12 p40 and Th17 cytokine IL-17 compared to wild-type animals (Fig. 1b, c). No Th2 cytokines (IL-4 and IL-10) were detectable in these cell types from either *Cryab*$^{-/-}$ or wild-type animals (not shown).

To determine the specific immune cells that were hyper-responsive during EAE in *Cryab*$^{-/-}$ mice, we assessed the proliferation capabilities and cytokine production of T cells and antigen-presenting cells such as macrophages and dendritic cells. CD3$^+$ T cells from *Cryab*$^{-/-}$ MOG-immunized mice stimulated with MOG proliferated more and secreted higher concentrations of IL-2, IFN-γ and IL-17 compared with their wild-type counterparts (Fig. 2a). Naive CD3$^+$ T cells from null animals also showed a similar hyper-responsiveness when stimulated in culture with anti-CD3 and anti-CD28 (not shown).

To assess whether antigen-presenting cell function was also affected, macrophages and dendritic cells from wild-type and *Cryab*$^{-/-}$ mice were stimulated with lipopolysaccharide (LPS).

[1]Department of Neurology and Neurological Sciences, Stanford University, [2]Division of Immunology and Rheumatology, Stanford University School of Medicine, Stanford, California 94305, USA. [3]GRECC and [7]Laboratory Service, Veterans Affairs Palo Alto Health Care System, Palo Alto, California 94304, USA. [4]Department of Biosciences, TNO Quality of Life, 2301 CE Leiden, The Netherlands. [5]National Eye Institute, National Institutes of Health, Bethesda, Maryland 20892, USA. [6]Center for Neurologic Disease, Harvard Medical School, Brigham and Women's Hospital, 77 Avenue Louis Pasteur, Boston, Massachusetts 02115, USA.

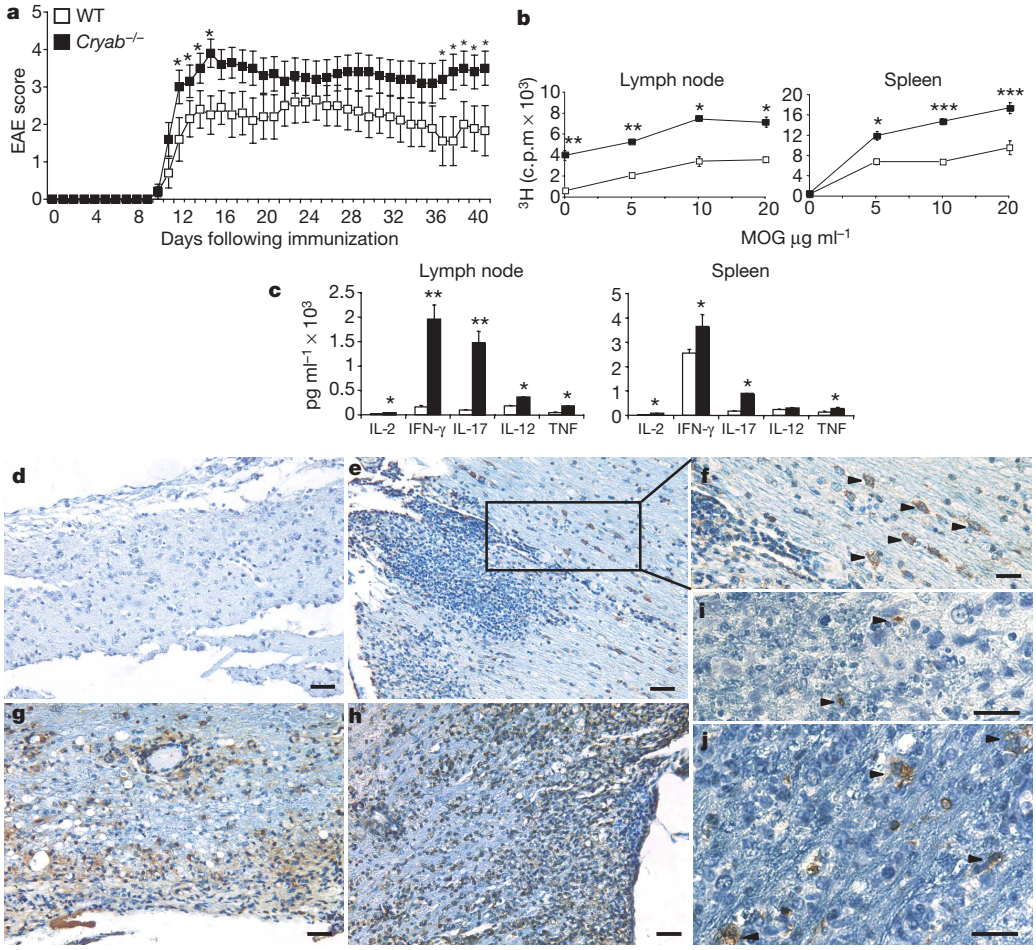

Figure 1 | Worse EAE, increased immune activation and glial apoptosis in *Cryab*$^{-/-}$ mice. Representatives from four EAE experiments show mean ± s.e.m. clinical scores of wild-type (WT) and *Cryab*$^{-/-}$ mice (**a**) (*$P < 0.05$ Mann–Whitney; $P = 0.0008$ linear regression days 9–15; $n = 10$ mice per group); and proliferation rate (**b**) and cytokine production (**c**) from wild-type and *Cryab*$^{-/-}$ (mean ± s.e.m.; *$P < 0.05$, **$P < 0.02$, ***$P < 0.005$, Student's *t*-test). **d–j**, Day 42 spinal cord from wild-type (**d**, **g**, **i**) and *Cryab*$^{-/-}$ (**e**, **f**, **h**, **j**) immuno-stained for cleaved (**d–f**) and uncleaved caspase-3 (**g**, **h**) and TUNEL (**i**, **j**). Arrows indicate glia. Scale bar, 200 μm (**d**, **e**, **g**, **h**) or 100 μm (**f**, **i**, **j**).

Null macrophages showed increased capacities to secrete inflammatory cytokines, releasing more IL-12 p40, IL-6 and IL-1β (Fig. 3a). These cells also secreted more IL-10, whereas there was no difference in TNF production. Similar to *Cryab*-deficient macrophages, LPS-stimulated *Cryab*$^{-/-}$ dendritic cells produced more IL-6, IL-12 p40 and TNF compared with wild-type cells (Supplementary Fig. 4). Wild-type dendritic cells on the other hand secreted more IL-1β.

To determine whether hyper-responsive immune cells from *Cryab*$^{-/-}$ mice contributed to either the inductive or the chronic phase of worsened EAE in *Cryab*-null animals, adoptive transfer experiments were performed. MOG-reactive splenocytes from wild-type and *Cryab*$^{-/-}$ immunized mice were injected into *Rag2*$^{-/-}$ mice. Significantly worse disease was observed in *Rag2*$^{-/-}$ recipients with *Cryab*$^{-/-}$ cells, but only in the acute phase of disease (Supplementary Fig. 5).

Because the MAP kinase signal transduction pathways are involved in Cryab function[12–14], we determined whether the JNK (c-Jun NH_2-terminal kinase), ERK (extracellular signal-regulated kinase) or p38 MAPK (p38 mitogen-activated protein kinase) pathways played a part in the immune cell hyper-responsiveness seen in *Cryab*$^{-/-}$ mice with EAE. We found that total and phosphorylated p38 expression was upregulated in stimulated *Cryab*$^{-/-}$ $CD3^+$ T cells (Fig. 2b and Supplementary Table 2) and macrophages (Fig. 3b and Supplementary Table 3). There was no difference in expression of the JNK and ERK pathway molecules between wild-type and *Cryab*$^{-/-}$ T cells and macrophages (not shown). These results demonstrated that the inflammatory response was hyperactive in *Cryab*$^{-/-}$ animals and

Table 1 | Quantification of inflammatory foci and TUNEL-positive (TUNEL$^+$) cells in brain and spinal cord samples of wild-type and *Cryab*$^{-/-}$ mice with EAE

	Meninges	Parenchyma	Total	TUNEL$^+$ parenchymal nuclei	TUNEL$^+$ glia
Day 14					
Wild-type	59 ± 17.6	49.5 ± 12.3	108.5 ± 29.1	145.7 ± 46.8	108.3 ± 38.7
Cryab$^{-/-}$	127.6 ± 17.7***	116.4 ± 7.2**	234 ± 17.7**	321.7 ± 56.1****	153.3 ± 40.9
Day 42					
Wild-type	20 ± 10.1	21 ± 11.1	41 ± 11.1	41 ± 13	3.5 ± 1.5
Cryab$^{-/-}$	135 ± 25.1*	151 ± 49.1****	286 ± 24.1*	275 ± 35.1*	142.5 ± 7.5*

Values are means ± s.e.m.; *$P < 0.05$, **$P < 0.01$, ***$P < 0.001$, ****$P = 0.06$; Student's *t*-test, $n = 4$ mice per group.

indicate that Cryab may have a dampening role on immune cell populations during EAE, though the dampening effect may be insufficient by itself to completely abrogate the disease.

Astrocytes use the canonical NF-κB pathway to modulate inflammation in EAE[15,16], and they upregulate expression of Cryab during EAE and multiple sclerosis[2]. We assessed whether the function of astrocytes is altered in *Cryab*$^{-/-}$ mice. Primary astrocytes isolated from *Cryab*$^{-/-}$ pups produced more IL-6 compared with wild-type astrocytes, 48 h following either TNF or staurosporine stimulation (Fig. 4a). Because Cryab is anti-apoptotic, we assessed whether *Cryab*$^{-/-}$ astrocytes underwent cell death at a different rate compared to wild-type astrocytes. Naive astrocytes from both wild-type and *Cryab*$^{-/-}$ mice expressed caspase-3 after four weeks in culture. However, naive and TNF-stimulated astrocytes from *Cryab*$^{-/-}$ mice showed differential levels of cleaved caspase-3 compared with wild-type cells, in which this apoptotic factor remained uncleaved even after stimulation with TNF (Fig. 4b). Furthermore, compared with wild-type cells a greater percentage of *Cryab*$^{-/-}$ astrocytes had more TUNEL staining with and without TNF stimulation (Fig. 4c), suggesting that Cryab protects astrocytes against normal cell death and during stress injury.

To determine the underlying signalling mechanism(s) mediating the increased cell death in the *Cryab*$^{-/-}$ astrocytes, we assessed the expression of the MAP kinase signal transduction pathways involved with Cryab function. Astrocytes from wild-type animals showed increased expression of Cryab 72h following TNF stimulation. These cells also showed a small increase in p-Cryab (Ser 59) levels but p-Cryab (Ser 45) decreased slightly (Fig. 4b). In terms of MAP kinase signalling, we found that ERK and p-ERK were upregulated in *Cryab*$^{-/-}$ astrocytes 72 h after TNF stimulation compared to wild-type astrocytes (Fig. 4b and Supplementary Table 4). p38 was also upregulated in null astrocytes after TNF stimulation, but the phosphorylated form of this protein was not detected. The levels of protein in TNF-stimulated astrocytes compared with media control also demonstrated an increase in p-ERK, ERK and p38 in *Cryab*$^{-/-}$ astrocytes. No changes in JNK and p-JNK expression were seen in wild-type and *Cryab*$^{-/-}$ astrocytes (not shown).

We then assessed whether the NF-κB pathway was modulated by Cryab. Astrocytes null for *Cryab* upregulated expression of the active subunits NF-κB p65 and NF-κB p105/p50 while down-regulating their negative regulator IκB-α, following TNF stimulation (Fig. 4b and Supplementary Table 4). Wild-type astrocytes on the other hand showed an increase in the IκB-α inhibitor and low NF-κB p50 was evident in total protein extracts in this genotype even after TNF stimulation (Fig. 4b). An assay for NF-κB DNA binding using nuclear extracts confirmed an enhancement in NF-κB p50 and NF-κB p65 DNA binding activity in null glia compared with wild-type cells (Fig. 4d). A small increase in NF-κB p50 DNA binding was seen in wild-type glia following TNF stimulation, but this level was much less than in activated *Cryab*$^{-/-}$ astrocytes (Fig. 4d). Therefore, Cryab probably prevents cell death of astrocytes by inhibiting caspase-3 activation, and suppresses the inflammatory role of NF-κB in astrocytes during demyelinating disease.

We have constructed large scale arrays to detect auto-antibodies to various myelin antigens, including full length CRYAB, and a number of its peptide epitopes[17]. In EAE, antibody to peptide regions, known as epitopes, p16–35, p26–45 and p116–135 on CRYAB appears within 17 days in the sera after immunization with PLPp139–151 (ref. 17). We applied these arrays to analyse antibody to CRYAB in the cerebrospinal fluid (CSF) of patients with relapsing remitting multiple sclerosis (RRMS). Antibodies to native CRYAB and to p21–40 and p116–135 of CRYAB were prominently detected compared to other neurological control (OND) patients (Fig. 5). We also detected free CRYAB in the serum and CSF of multiple sclerosis patients (Supplementary Fig. 7).

Our results indicated that CRYAB has both a suppressive effect on immunity and an anti-apoptotic role in glia. To show that antibody to CRYAB from the CSF of multiple sclerosis patients worsened EAE would be complicated by the fact that in EAE there are already antibodies to CRYAB that arise from epitope spreading[18], as we and others have shown earlier[17,19]. We therefore assessed whether recombinant CRYAB itself could resolve ongoing EAE. To test this, we

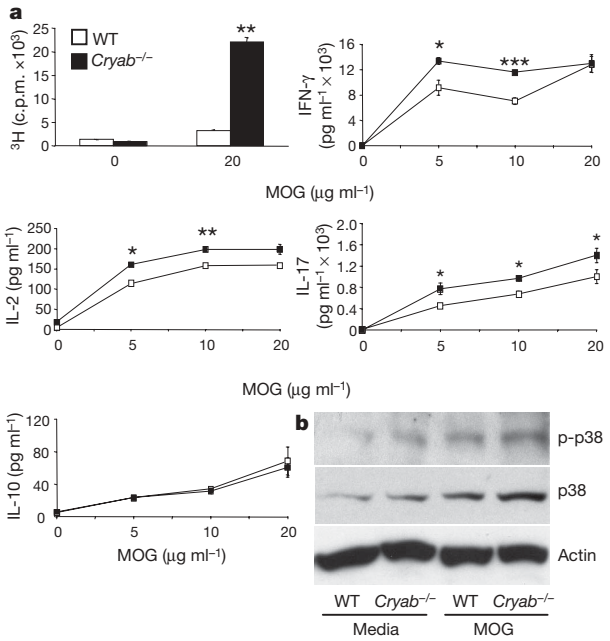

Figure 2 | T cells from *Cryab*$^{-/-}$ EAE mice are hyper-responsive. **a**, Representative graphs from three experiments showing proliferation rate (c.p.m.) and secretion of Th1 (IFN-γ, IL-2), Th17 (IL-17) and Th2 (IL-10) cytokines (pg ml^{-1}) from CD3^{+} T cells isolated from wild-type and *Cryab*$^{-/-}$ EAE mice and stimulated with syngeneic irradiated splenocytes and MOG 35–55; mean ± s.e.m.; $^{*}P < 0.05$, $^{**}P < 0.02$, $^{***}P < 0.001$, Student's *t*-test. **b**, Representative western blots from two separate experiments showing p38 and phospho-p38 (p-p38) expression in CD3^{+} T cells from wild-type and *Cryab*$^{-/-}$ EAE mice stimulated with syngeneic irradiated splenocytes and MOG 35–55 peptide for 1 h.

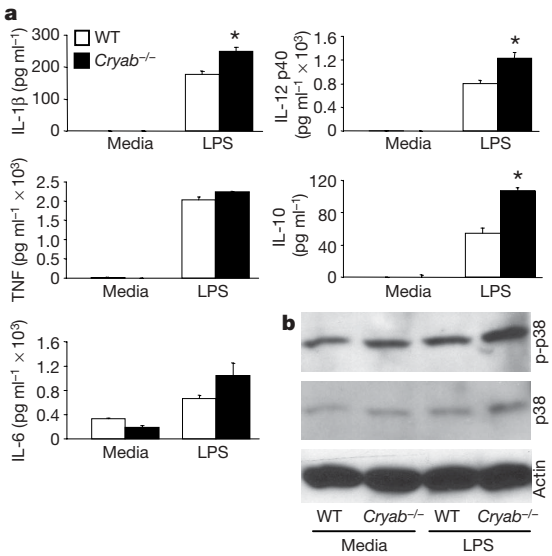

Figure 3 | Macrophages deficient in *Cryab* are hyperactive. **a**, Representative graphs from three experiments showing production of cytokines (IL-1β, TNF, IL-6, IL-12 p40, IL-10) by wild-type and *Cryab*$^{-/-}$ macrophages stimulated *in vitro* with LPS; mean ± s.e.m., $^{*}P < 0.05$ Student's *t*-test. **b**, Representative western blot from two separate experiments showing p38 and phospho-p38 (p-p38) expression in wild-type and *Cryab*-null macrophages 72 h after stimulation with LPS.

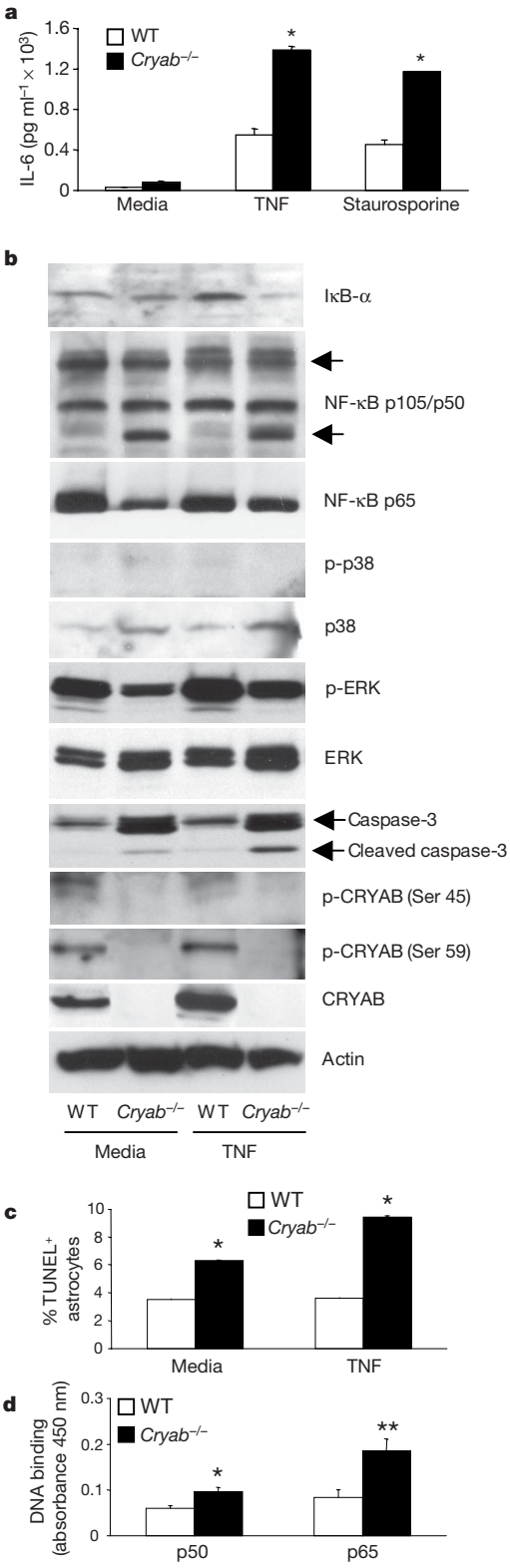

Figure 4 | *Cryab*$^{-/-}$ astrocytes are more susceptible to cell death and augment ERK and NF-κB signalling. **a**, IL-6 production by wild-type and *Cryab*$^{-/-}$ astrocytes 48 h post-TNF stimulation; $^*P < 0.03$, mean ± s.e.m. **b**, Representative blots from two experiments showing Cryab, phospho-Cryab, cleaved and uncleaved caspase-3, p38, phospho-p38, ERK, phospho-ERK, NF-κB p105/p50, p65 and IκB-α levels in wild-type and *Cryab*$^{-/-}$ astrocytes 72 h post TNF stimulation. **c**, Mean ± s.e.m. of percentages of TUNEL$^+$ astrocytes after 72 h with TNF; $^*P < 0.005$. **d**, Mean ± s.e.m. of DNA binding of NF-κB p50 and p65 in wild-type and *Cryab*$^{-/-}$ astrocytes 72 h post TNF stimulation; $^*P = 0.067$, $^{**}P = 0.017$, all *P* values by Student's *t*-test.

treated wild-type 129S6 mice with EAE with recombinant human CRYAB, administered intravenously. Mice treated with CRYAB showed significantly lower clinical disease scores compared with animals injected with PBS or an inert protein control, recombinant human myoglobin (Fig. 6a, b). PBS and myoglobin were similar in their inability to influence clinical EAE. *Cryab*$^{-/-}$ and SJL/J mice with EAE were also successfully treated with recombinant CRYAB (Supplementary Fig. 6a, b). The amelioration of disease by CRYAB in 129S6 mice was in part due to decreased infiltration of immune cells into the brain and spinal cord (Table 2) and suppression of immune cell function (Fig. 6b). We observed decreased proliferation and diminished production of IL-2, IL-12 p40, TNF, IFN-γ and IL-17 cytokines by splenocytes taken from mice treated with recombinant CRYAB (Fig. 6b). Interestingly, increased production of the immune suppressive cytokine, IL-10, was observed at high concentrations of MOG stimulation (Fig. 6b). A decrease in immune cell function was similarly observed in CD3$^+$ T cells stimulated *in vitro* with anti-CD3/anti-CD28 and treated with recombinant CRYAB (not shown).

To assess whether recombinant CRYAB treatment affected cell death in the CNS we performed TUNEL-staining on brain and spinal cord sections from PBS and CRYAB-treated EAE mice. Less TUNEL staining was observed in CNS parenchyma in mice treated with CRYAB compared to PBS-injected animals (Table 2; Supplementary Fig. 3). In addition, fewer TUNEL-positive cells with diffuse cytoplasmic staining suggestive of dying glial cells were seen in the CNS of crystallin-treated animals, suggesting a protective effect on glia by exogenously administered recombinant CRYAB.

Other mechanisms of CRYAB therapy are being investigated, such as whether recombinant CRYAB could bind to or traverse across plasma membranes[20] or neutralize CRYAB antibodies akin to strategies in Alzheimer's disease[21,22].

One of the main adaptive immunological responses in multiple sclerosis and its animal model, EAE, is thus directed to an inducible stress protein, CRYAB. Such an immune response targeting a negative regulator of brain inflammation thus disrupting its function[23,24], is comparable to damaging the braking system of a vehicle that is already careening into danger. Remarkably, addition of that very same stress protein, akin to restoring the brakes that were failing,

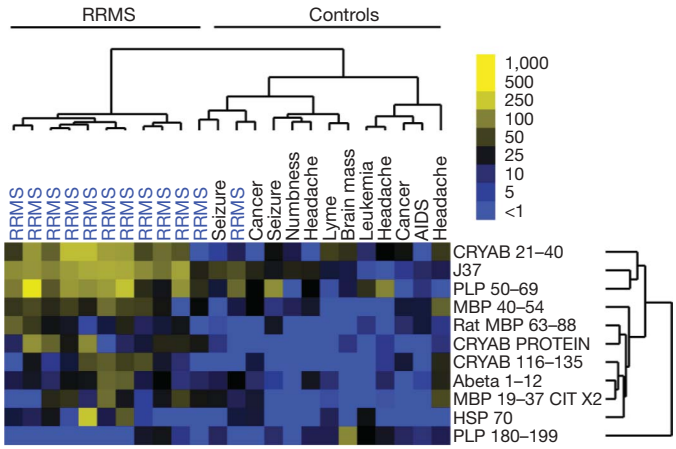

Figure 5 | Myelin antigen array analysis demonstrates antibody targeting of CRYAB in RRMS patients. Analysis was performed on CSF from RRMS and OND patients. Statistical analysis of microarrays (SAM) identified significant differences in antibodies in RRMS compared with OND. Samples are arranged with hierarchical clustering, and displayed as a heat map. RRMS patients demonstrated significantly increased auto-antibodies against various myelin epitopes including CRYAB protein and peptides (J37, Golli-myelin basic protein isoform J37); PLP, proteolipid protein; MBP, myelin basic protein; HSP, heat shock protein; Abeta, amyloid beta). A false discovery rate threshold of 1.9% and numerator threshold of 2.0 were used. Prediction analysis of microarrays (PAM) yielded a classification model with 21 markers, with cross-validated sensitivity of 10/12 = 83% and specificity of 11/12 = 92%.

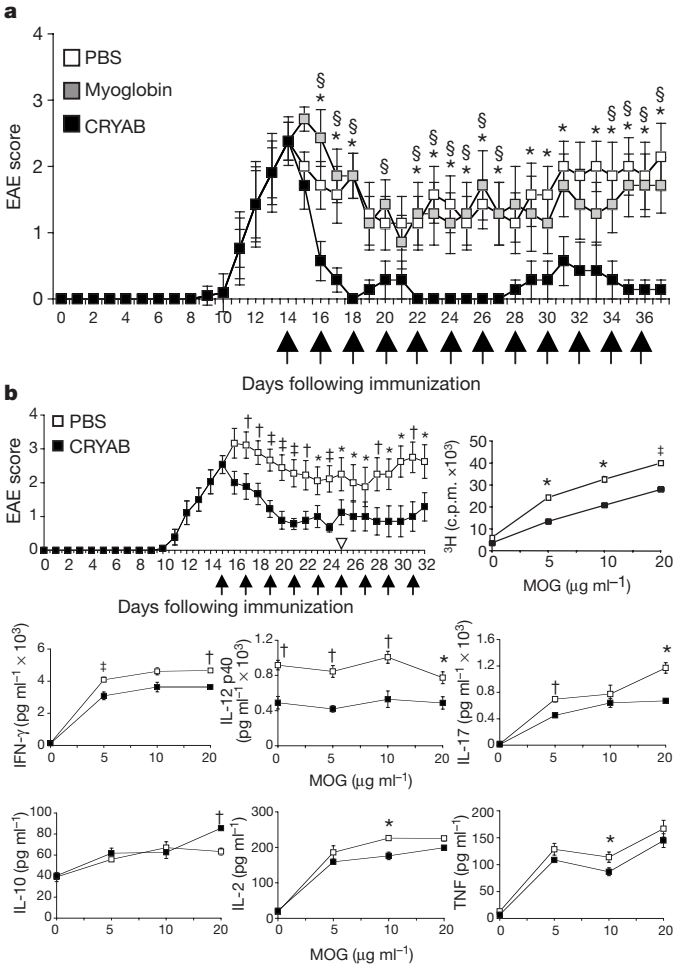

Figure 6 | CRYAB suppresses disease and inflammation in EAE. **a**, Representative graph from three experiments showing mean ± s.e.m. scores of 129S6 EAE mice treated with CRYAB, PBS or myoglobin. Treatment indicated with arrows. §*$P < 0.05$ Mann–Whitney, §CRYAB versus myoglobin, *CRYAB versus PBS; linear regression (CRYAB versus PBS, $P = 0.0011$; CRYAB versus myoglobin, $P = 0.038$), days 13–22; $n = 10$ mice per group. **b**, Proliferation rate (c.p.m.) and cytokine production (pg ml^{-1}) of splenocytes at day 25 (white arrow head) of EAE during CRYAB or PBS treatment. EAE: *$P < 0.05$, †$P < 0.01$ Mann–Whitney; $P = 0.0258$ linear regression ($n = 10$ mice per group); proliferation and cytokine: *$P < 0.05$, †$P < 0.01$, ‡$P < 0.005$, Student's *t*-test.

returns control. CRYAB, a negative regulator of inflammation in EAE and multiple sclerosis brain, and a potent modulator of glial apoptosis, is apparently located at a critical tipping point in the pathophysiology of multiple sclerosis.

METHODS

EAE. EAE was induced in *Cryab*-null (*Cryab*$^{-/-}$) and wild-type 129S6/SvEvTac mice with myelin oligodendrocyte glycoprotein (MOG p35–55) and *Bordetella pertussis* toxin. Clinical disease was scored as followed: 0, no disease; 1, limp tail; 2, hindlimb weakness; 3, complete hindlimb paralysis; 4, hindlimb paralysis plus forelimb paralysis; and 5, moribund or dead. For recombinant CRYAB treatment, EAE mice were injected intravenously every second day with saline, 10 μg recombinant human CRYAB or 10 μg recombinant human myoglobin. Paraffin-embedded brain and spinal cords were processed for histological analysis and apoptosis detection.

Cell activation. Splenocytes, lymph node cells, CD3$^+$ T cells, primary macrophages, dendritic cells or astrocytes were stimulated with MOG, LPS or TNF. Proliferation rates were determined by [^{3}H]-thymidine incorporation and cytokine secretion assessed by enzyme-linked immunosorbent assay (ELISA).

Western blot. CD3$^+$ T cells, macrophages and astrocytes protein lysates were subjected to SDS–PAGE electrophoresis. Proteins were transferred to PVDF membranes and immunoblotted with various CRYAB, caspase-3, MAP kinase and NF-κB antibodies. Bound antibodies were visualized by enhanced chemiluminescence.

Table 2 | Quantification of inflammatory foci and TUNEL-positive (TUNEL$^+$) cells in brain and spinal cord samples of wild-type mice with EAE treated with PBS or recombinant human CRYAB

	Meninges	Parenchyma	Total	TUNEL$^+$
PBS	115.3 ± 31.8	107.7 ± 28.3	223 ± 60.1	487.1 ± 104.1
Recombinant CRYAB	48.7 ± 19.8*	52 ± 38.5*	100.7 ± 55.8**	152.7 ± 74*

Values are means ± s.e.m.; *$P < 0.03$, **$P < 0.005$; Student's *t*-test, $n = 3$ mice per group.

Myelin arrays. Proteins and peptides representing candidate myelin autoantigens were printed in ordered arrays on the surface of SuperEpoxy microscope slides. Myelin arrays were probed with 1:20 dilutions of cerebrospinal fluid derived from relapsing remitting multiple sclerosis or other neurologic disease control patients, followed by Cy-3-conjugated anti-human IgG/M secondary antibody. Arrays were scanned, and fluorescence quantified as a measure of auto-antibody binding[17].

Statistical analysis. Data are presented as means ± s.e.m. EAE results were analysed by Mann–Whitney statistics and linear regression, whereas proliferation rate, cytokine production, histological analysis and densitometry were assessed by Student's *t*-test. Myelin array results were analysed using Significance Analysis of Microarrays (SAM)[25] and Prediction Analysis of Microarrays (PAM).

A detailed description of the materials and methods is described in Methods.

Full Methods and any associated references are available in the online version of the paper at www.nature.com/nature.

Received 6 March; accepted 17 May 2007.
Published online 13 June 2007.

1. Chabas, D. *et al.* The influence of the proinflammatory cytokine, osteopontin, on autoimmune demyelinating disease. *Science* **294**, 1731–1735 (2001).
2. Aoyama, A., Frohli, E., Schafer, R. & Klemenz, R. αB-crystallin expression in mouse NIH 3T3 fibroblasts: glucocorticoid responsiveness and involvement in thermal protection. *Mol. Cell. Biol.* **13**, 1824–1835 (1993).
3. Mao, Y. W. *et al.* Human *bcl-2* gene attenuates the ability of rabbit lens epithelial cells against H_2O_2-induced apoptosis through down-regulation of the alpha B-crystallin gene. *J. Biol. Chem.* **276**, 43435–43445 (2001).
4. Dasgupta, S., Hohman, T. C. & Carper, D. Hypertonic stress induces alpha B-crystallin expression. *Exp. Eye Res.* **54**, 461–470 (1992).
5. Mehlen, P., Kretz-Remy, C., Preville, X. & Arrigo, A. P. Human hsp27, *Drosophila* hsp27 and human alphaB-crystallin expression-mediated increase in glutathione is essential for the protective activity of these proteins against TNFalpha-induced cell death. *EMBO J.* **15**, 2695–2706 (1996).
6. Andley, U. P., Song, Z., Wawrousek, E. F., Fleming, T. P. & Bassnett, S. Differential protective activity of alpha A- and alphaB-crystallin in lens epithelial cells. *J. Biol. Chem.* **275**, 36823–36831 (2000).
7. Li, D. W. *et al.* Caspase-3 is actively involved in okadaic acid-induced lens epithelial cell apoptosis. *Exp. Cell Res.* **266**, 279–291 (2001).
8. Masilamoni, J. G. *et al.* Molecular chaperone alpha-crystallin prevents detrimental effects of neuroinflammation. *Biochim. Biophys. Acta* **1762**, 284–293 (2006).
9. van Noort, J. M. *et al.* The small heat-shock protein αB-crystallin as candidate autoantigen in multiple sclerosis. *Nature* **375**, 798–801 (1995).
10. Bajramovic, J. J. *et al.* Presentation of alpha B-crystallin to T cells in active multiple sclerosis lesions: an early event following inflammatory demyelination. *J. Immunol.* **164**, 4359–4366 (2000).
11. Kamradt, M. C., Chen, F., Sam, S. & Cryns, V. L. The small heat shock protein alpha B-crystallin negatively regulates apoptosis during myogenic differentiation by inhibiting caspase-3 activation. *J. Biol. Chem.* **277**, 38731–38736 (2002).
12. Morrison, L. E., Hoover, H. E., Thuerauf, D. J. & Glembotski, C. C. Mimicking phosphorylation of alphaB-crystallin on serine-59 is necessary and sufficient to provide maximal protection of cardiac myocytes from apoptosis. *Circ. Res.* **92**, 203–211 (2003).
13. Webster, K. A. Serine phosphorylation and suppression of apoptosis by the small heat shock protein alphaB-crystallin. *Circ. Res.* **92**, 130–132 (2003).
14. Liu, J. P. *et al.* Human alphaA- and alphaB-crystallins prevent UVA-induced apoptosis through regulation of PKCalpha, RAF/MEK/ERK and AKT signaling pathways. *Exp. Eye Res.* **79**, 393–403 (2004).
15. van Loo, G. *et al.* Inhibition of transcription factor NF-κB in the central nervous system ameliorates autoimmune encephalomyelitis in mice. *Nature Immunol.* **7**, 954–961 (2006).
16. Youssef, S. & Steinman, L. At once harmful and beneficial: the dual properties of NF-κB. *Nature Immunol.* **7**, 901–902 (2006).
17. Robinson, W. H. *et al.* Protein microarrays guide tolerizing DNA vaccine treatment of autoimmune encephalomyelitis. *Nature Biotechnol.* **21**, 1033–1039 (2003).
18. Ellmerich, S. *et al.* Disease-related epitope spread in a humanized T cell receptor transgenic model of multiple sclerosis. *Eur. J. Immunol.* **34**, 1839–1848 (2004).

19. van Noort, J. M., Verbeek, R., Meilof, J. F., Polman, C. H. & Amor, S. Autoantibodies against alpha B-crystallin, a candidate autoantigen in multiple sclerosis, are part of a normal human immune repertoire. *Mult. Scler.* **12,** 287–293 (2006).
20. Cobb, B. A. & Petrash, J. M. Characterization of alpha-crystallin-plasma membrane binding. *J. Biol. Chem.* **275,** 6664–6672 (2000).
21. Matsuoka, Y. *et al.* Novel therapeutic approach for the treatment of Alzheimer's disease by peripheral administration of agents with an affinity to β-amyloid. *J. Neurosci.* **23,** 29–33 (2003).
22. Bard, F. *et al.* Peripherally administered antibodies against amyloid β-peptide enter the central nervous system and reduce pathology in a mouse model of Alzheimer disease. *Nature Med.* **6,** 916–919 (2000).
23. Korlimbinis, A., Hains, P. G., Truscott, R. J. & Aquilina, J. A. 3-Hydroxykynurenine oxidizes alpha-crystallin: potential role in cataractogenesis. *Biochemistry* **45,** 1852–1860 (2006).
24. Finley, E. L., Dillon, J., Crouch, R. K. & Schey, K. L. Identification of tryptophan oxidation products in bovine alpha-crystallin. *Protein Sci.* **7,** 2391–2397 (1998).
25. Tusher, V. G., Tibshirani, R. & Chu, G. Significance analysis of microarrays applied to the ionizing radiation response. *Proc. Natl Acad. Sci. USA* **98,** 5116–5121 (2001).

Supplementary Information is linked to the online version of the paper at www.nature.com/nature.

Acknowledgements This research was supported by NIH and National Multiple Sclerosis Society (NMSS) grants to L.S. and fellowships to S.S.O. from the NMSS and Multiple Sclerosis Society of Canada (MSSC). We thank R. Tibshirani for his advice on statistical analysis.

Author Contributions S.S.O. and L.S. formulated the hypothesis and aims and designed all experiments. W.H.R. and B.H.T. did the myelin array experiment. D.A.H. and K.O'C. provided multiple sclerosis CSF for the myelin array. R.A.S. analysed and quantified the EAE and astrocyte histology. J.M.V.N. provided the CRYAB human protein construct for the myelin array and performed the western blot for CRYAB in multiple sclerosis sera and CSF. E.F.W. developed and provided the *Cryab*$^{-/-}$ mice.

Author Information Reprints and permissions information is available at www.nature.com/reprints. The authors declare no competing financial interests. Correspondence and requests for materials should be addressed to L.S. (steinman@stanford.edu).

METHODS

Mice. *Cryab*-null mice ($Cryab^{-/-}$) were developed at the NIH National Eye Institute[26]. These mice were generated from embryonic stem cells with a 129S4/SvJae background and maintained in 129S6/SvEvTac × 129S4/SvJae background. $Cryab^{-/-}$ mice are viable and fertile, with no obvious prenatal defects and normal lens transparency. Older mice show postural defects and progressive myopathy that are apparent at approximately 40 weeks of age[26]. We studied these mice between 8–12 weeks thus removing the possible effects of myopathy on our clinical evaluation. The $Cryab^{-/-}$ mice also have a deletion of the related gene, *Hspb2*. It is unlikely that deletion of the *Hspb2* gene would have any effects on the immunological or neurobiological processes involved in this study, primarily because it is not normally expressed in brain and in any lymphoid cell[27]. Also, *Hspb2* is not heat-shock-inducible, unlike *Cryab*, and is thus unlikely to act as a general 'chaperone'[27,28]. We therefore attribute the effects observed to Cryab deficiency only, and not to Hspb2 deficiency. 129S6/SvEvTac (Taconic Farms) mice were used as controls. Colonies of wild-type and $Cryab^{-/-}$ mice were maintained in our animal colony and bred according to Stanford University Comparative Medicine guidelines. SJL/J mice were purchased from Jackson Laboratories, Bar Harbor, Maine.

EAE induction. EAE was induced in 8–12-week-old female mice via subcutaneous immunization with 100 μg myelin oligodendrocyte glycoprotein (MOG p35–55) ($Cryab^{-/-}$ and wild-type 129S6/SvEvTac animals) or proteolipid protein (PLP 139–151) (SJL/J) peptide in an emulsion mixed (volume ratio 1:1) with Complete Freund's Adjuvant (CFA) (containing 4 mg ml^{-1} of heat-killed *Mycobacterium tuberculosis* H37Ra, Difco Laboratories). MOG-immunized $Cryab^{-/-}$ and wild-type 129S6/SvEvTac animals were additionally injected intravenously with 50 ng of *Bordetella pertussis* toxin (Difco Laboratories) in PBS at the time of, and two days following immunization. MOG p35–55 and PLP 139–151 peptides were synthesized by the Stanford Pan Facility and purified by high performance liquid chromatography (HPLC). Mice ($n = 8$–10 per group) were examined daily for clinical signs of EAE and were scored. All animal protocols were approved by the Division of Comparative Medicine at Stanford University and animals were maintained in accordance with the guidelines of the National Institutes of Health.

Adoptive transfer. Female, 8–12-week-old $Cryab^{-/-}$ and wild-type 129S6/SvEvTac animals were immunized with 100 μg myelin oligodendrocyte glycoprotein (MOG p35–55) peptide in CFA (containing 4 mg ml^{-1} of heat-killed *Mycobacterium tuberculosis* H37Ra, Difco Laboratories) along with 50 ng of *Bordetella pertussis* toxin (Difco Laboratories) in PBS administered intravenously at days 0 and 2 following immunization. Splenocytes were isolated at day 10 following immunization and cultured in the presence of 20 μg ml^{-1} MOG 35–55 and 20 ng ml^{-1} murine rIL-12 (R&D Systems). Cells were collected and washed in PBS after 4 days in culture. Living (2×10^7) wild-type and $Cryab^{-/-}$ cells were intravenously injected into female $Rag2^{-/-}$ mice (Taconic Farms). Animals were also injected intravenously with 50 ng *pertussis* toxin on the day of, and 48 h after cell transfer[29].

Histopathology. Brains and spinal cords were dissected from mice, fixed in 10% formalin in PBS and embedded in paraffin. Seven-micron-thick sections were stained with haematoxylin and eosin to detect inflammatory infiltrates and luxol fast blue for demyelination. Inflammatory foci (greater than 10 inflammatory cells per focus) were counted in meninges and parenchyma of sections containing brain, thoracic and lumbar spinal cord from each mouse by an examiner masked to the treatment status of the animal.

Astrocyte culture. Astrocytes were derived from the brains of 2-day-old $Cryab^{-/-}$ and wild-type pups. Briefly, the cerebral cortices from three pups of each genotype were dissected and placed in modified Dulbecco's modified Eagle's medium (DMEM, Invitrogen) containing penicillin-streptomycin-L-glutamine (Invitrogen). The meninges were removed and the cortices placed in 1 ml of complete DMEM containing 10% fetal bovine serum, 2 mM L-glutamine, 1 mM sodium pyruvate, 0.1 mM non-essential amino acids, 100 U ml^{-1} penicillin and 0.1 mg ml^{-1} streptomycin (Invitrogen). The cortices were minced, vortexed at high speed for 1 min, and passed though an 18.5-gauge needle. The ensuing mixture was filtered successively through sterile 80-μm and 11-μm nylon filters (Millipore) using a 25-mm Swinnex syringe filter holder (Millipore). The filtered cells were then diluted up to 1 ml with complete DMEM, plated into three 75-cm^2 tissue culture flasks containing 10 ml of complete DMEM, and placed in a 5% aerated CO_2 incubator kept at 37 °C. After 10–12 days in culture flasks, cells were shaken at 250 r.p.m. for two hours at 37 °C to remove microglia, fibroblasts or endothelial cells. Confluent astrocytes were stimulated with 200 ng ml^{-1} recombinant TNF (BioSource) or 100 nM staurosporine (Sigma) and the cells and supernatants harvested for ELISA and western blot analysis following stimulation. Astrocytes were also grown on glass coverslips, stimulated with 200 ng ml^{-1} recombinant TNF and stained for apoptosing cells using the TUNEL technique (described below).

Immune cell activation assays and cytokine analysis. Splenocytes and lymph node cells (5×10^5 cells/well) or CD3$^+$ T cells (5×10^4 cells per well; purified by negative selection, R&D Systems) were cultured in flat-bottomed, 96-well plates in media (RPMI 1640 supplemented with 2 mM L-glutamine, 1 mM sodium pyruvate, 0.1 mM non-essential amino acids, 100 U ml^{-1} penicillin, 0.1 mg ml^{-1} streptomycin, 0.5 μM 2-mercaptoethanol and 10% fetal calf serum) with MOG p35–55 peptide (5–20 μg ml^{-1}). To determine *in vivo* T-cell function CD3$^+$ T cells were purified from the spleens and lymph nodes of day 9 MOG-immunized mice and cultured 1:5 with irradiated syngeneic splenocytes and MOG p35–55 peptide (5–20 μg ml^{-1}).

Primary macrophages were isolated from the peritoneal cavity of $Cryab^{-/-}$ and wild-type mice 3 days after intraperitoneal injection with 3 ml of 3% (w/v) thioglycollate (BD Diagnostics Systems) and cultured (1×10^6 cells ml^{-1}) with media alone (DMEM supplemented with 10% FCS, 1 mM sodium pyruvate, 100 U ml^{-1} penicillin, and 0.1 mg ml^{-1} streptomycin) in 24-well plates for 72 h and then activated with 100 ng ml^{-1} of LPS.

Primary dendritic cells were isolated from the spleens of naive $Cryab^{-/-}$ and wild-type animals by magnetic cell sorting according to the manufacturer's directions for the CD11c *MACS* dendritic cell kit (Miltenyi Biotec). Dendritic cells (1×10^6 cells ml^{-1}) were cultured in DMEM containing 10% FCS, 100 U ml^{-1} penicillin, and 0.1 mg ml^{-1} streptomycin in 24-well plates and pulsed with 100 ng ml^{-1} LPS for 1 h, 24 h, 48 h and 72 h.

To assess proliferation rate, cultures were pulsed with [^{3}H]-thymidine (1 μCi per well) after 72 h of culture and harvested 18 h later onto filter paper. The counts per minute (c.p.m.) of incorporated [^{3}H]-thymidine were read using a beta counter. Cytokines were measured in the supernatants of cultured cells using anti-mouse OPTEIA ELISA kits (BD Pharmingen). Supernatants were taken at the time of peak production for each cytokine (48 h: IL-2, IL-12 p40, IL-6, IL-1β; 72h: IFN-γ, TNF; 96 h: IL-17; 120h: IL-4, IL-10). For all activation assays, cells were pooled from three animals per group and triplicate wells plated.

Recombinant CRYAB treatment. 129S6, $Cryab^{-/-}$, and SJL/J mice were induced with EAE using 100 μg MOG p35–55 (for 129S6 and $Cryab^{-/-}$) or 100 μg PLP 139–151 (for SJL/J) peptide emulsified in CFA. 129S6 and $Cryab^{-/-}$ mice were also injected intravenously with 50 ng of *Bordetella pertussis* toxin (Difco Laboratories) in PBS at the time of, and two days following immunization. When mice had hindlimb paralysis animals were divided into three groups balanced for mean clinical disease scores, and then injected intravenously every second day with saline pH 7.0, 10 μg recombinant human CRYAB (US Biological) or 10 μg recombinant human myoglobin (US Biological) diluted in saline. To determine the effect of CRYAB treatment on immune cell function during EAE splenocytes from 129S6 mice were isolated during the remission phase, and stimulated *in vitro* with MOG 35–55 (5-20 μg ml^{-1}). Proliferation rate was determined by [^{3}H]-thymidine (1 μCi per well) incorporation after 72 h of culture, whereas cytokines were measured in the supernatants at the time of their peak production (48 h: IL-2, IL-12 p40, IL-6, IL-1β; 72h: IFN-γ, TNF; 96 h: IL-17; 120h: IL-4, IL-10). Brains and spinal cords were harvested at the end of the experiment, embedded in paraffin and sections processed for histological analysis and TUNEL staining.

Western blot analysis. CD3$^+$ T cells, macrophages and astrocytes were lysed in 50 mM Tris–HCl buffer, pH 7.4, containing 1% NP-40, 10% glycerol, 1 mM EDTA, 1 mM Na_3VO_4, 1 mM NaF, 1 mM DTT, 4.5 mM Na pyrophosphate, 10 mM β-glycerophosphate, and a protease inhibitor cocktail tablet (Roche Diagnostics). The supernatants were collected after centrifugation at 13,000 r.p.m. at 4 °C for 30 min, and protein content determined with a spectrophotometer using absorption at 280 nm. Protein lysates (30–50 μg) were suspended in two volumes of double-strength sodium dodecyl sulphate (SDS) Sample Buffer (Bio-Rad Laboratories) and subjected to SDS–polyacrylamide gel electrophoresis using 10 or 15% Tris-HCl Ready Gels (Bio-Rad Laboratories). Proteins were transferred to PVDF membranes and blocked with 5% non-fat dried milk in 20 mM Tris–HCl-buffered saline (TBS), pH 7.4, containing 0.05% Tween-20. Membranes were immunoblotted 1:500 with the following antibodies overnight at 4 °C: p-CRYAB (Ser 45), p-CRYAB (Ser 59), CRYAB (StressGen BioReagents); actin (Sigma); p-p38, p38, p-ERK, ERK, p-SAPK/JNK, SAPK/JNK, caspase-3, NFκB p105/p50, NF-κB p65, IκB-α (Cell Signalling Technology). Membranes were washed three times for 15 min with TBS buffer containing 0.1% Tween-20. Bound antibodies were visualized using peroxidase-conjugated secondary antibody (Amersham) followed by detection using an ECL kit (Pierce). For reblotting, the membrane was first stripped in buffer (62.5 mM Tris–HCl, pH 6.8, with 2% SDS and 100 mM β-mercaptoethanol) for 1 h at 50 °C.

Immunohistochemistry. Paraffin-embedded sagittal sections (7 μm) were hydrated and treated for antigen retrieval using 10 mM sodium citrate. Sections were incubated in 1% hydrogen peroxide to quench endogenous peroxidase, blocked in 1% BSA in PBS for 1 h at room temperature, and incubated

overnight at 4 °C with caspase-3 (1:50) or cleaved caspase-3 (1:400) (Cell Signaling). Bound antibody was detected using Vectastain ABC anti-rabbit kits (Vector Laboratories) and 3,5-diaminobenzidine (DAB)/H_2O_2 reagent as substrate. Before mounting, sections were counterstained with Mayer's haematoxylin and dehydrated in graded ethanols. To detect for apoptosis using the TUNEL method, we used the ApopTag peroxidase *in situ* apoptosis detection kit according to the manufacturer's directions for paraffin-embedded sections (Chemicon). TUNEL-positive small, round parenchymal cells and larger glia were counted in CNS tissue from representative mice. For astrocyte cultures, proportions of TUNEL-positive cells in fifty randomly selected fields per slide were quantified.

NF-κB binding assay. Wild-type and *Cryab*$^{-/-}$ astrocytes were stimulated with 200 ng ml^{-1} TNF (BioSource) for 72 h and nuclear protein extracts isolated using Clontech Laboratories' Transfactor Extraction kit. NF-κB p50 and NF-κB DNA binding was detected with 15 μg of nuclear protein using Clontech Transfactor Family Colorimetric kit-NF-κB.

Myelin arrays. Myelin antigen arrays were printed and probed as previously described[17]. Briefly, proteins and peptides representing candidate myelin auto-antigens were printed in ordered arrays on the surface of SuperEpoxy microscope slides (TeleChem). Myelin arrays were probed with 1:20 dilutions of cerebrospinal fluid (CSF) derived from relapsing remitting multiple sclerosis (RRMS) or other neurologic disease (OND) control patients, followed by Cy-3-conjugated anti-human IgG/M secondary antibody (Jackson Immunoresearch). Arrays were scanned, and fluorescence quantified as a measure of auto-antibody binding.

Measurement of free CRYAB in sera and CSF. Paired post-mortem samples of CSF (0.5 mL) and serum (1.0 mL) of clinically definite, and neuropathologically confirmed multiple sclerosis patients were subjected to denaturation by 1:10 dilution in 8 M urea and 2% (vol/vol) acetic acid and left at room temperature for 1 h to disrupt all possible immune complexes. Samples were next applied onto a reversed-phase HPLC column (C4 matrix, 5 micron particle size, 250 Å pores) and washed with 0.1% (vol/vol) trifluoroacetic acid (TFA) in water, containing 25% acetonitrile. In a final step, any CRYAB in the samples was eluted from the column with 45% acetonitrile in 0.1% TFA (CRYAB elutes at 37% acetonitrile under these conditions) and the eluate was lyophilized. Dried proteins were redissolved in 120 ml (CSF) and 500 ml (serum) and 20 ml of these samples were subjected to SDS–PAGE and western blotting using a monoclonal antibody to CRYAB. Thus, CSF samples were concentrated about 4 times, and serum 2 times. Human recombinant CRYAB (0.4 mg) was used as a reference.

Western blot densitometric quantification. Western blot bands were quantified using NIH Image Analysis 1.63 software. Briefly, arbitrary pixel units were obtained for an area around each band and the optical density (OD) within that area. A ratio of OD:area was derived for each band. The OD:area values for a protein of interest were then normalized to the corresponding actin OD:area values.

Statistical analysis. Data are presented as means ± s.e.m. When data were parametric a *t*-test ($n = 2$ groups) was used to detect between-group differences. When data were non-parametric, Mann–Whitney U statistics were used for $n = 2$ groups. Clinical results when measured on a daily basis were compared with linear regression analysis in a pairwise comparison with either PBS or myoglobin or both controls. Myelin array results were analysed using Significance Analysis of Microarrays (SAM)[25] to identify antigen features with significant differences in antibody reactivity. These antigen 'hits' and the patient samples were then ordered using a hierarchical clustering algorithm and the results displayed as a heat map using TreeView software[30].

26. Brady, J. P. *et al.* αB-crystallin in lens development and muscle integrity: a gene knockout approach. *Invest. Ophthalmol. Vis. Sci.* **42**, 2924–2934 (2001).
27. Suzuki, A. *et al.* MKBP, a novel member of the small heat shock protein family, binds and activates the myotonic dystrophy protein kinase. *J. Cell Biol.* **140**, 1113–1124 (1998).
28. Doerwald, L. *et al.* Sequence and functional conservation of the intergenic region between the head-to-head genes encoding the small heat shock proteins αB-crystallin and HspB2 in the mammalian lineage. *J. Mol. Evol.* **59**, 674–686 (2004).
29. Huang, D. R., Wang, J., Kivisakk, P., Rollins, B. J. & Ransohoff, R. M. Absence of monocyte chemoattractant protein 1 in mice leads to decreased local macrophage recruitment and antigen-specific T helper cell type 1 immune response in experimental autoimmune encephalomyelitis. *J. Exp. Med.* **193**, 713–726 (2001).
30. Eisen, M. B., Spellman, P. T., Brown, P. O. & Botstein, D. Cluster analysis and display of genome-wide expression patterns. *Proc. Natl Acad. Sci. USA* **95**, 14863–14868 (1998).